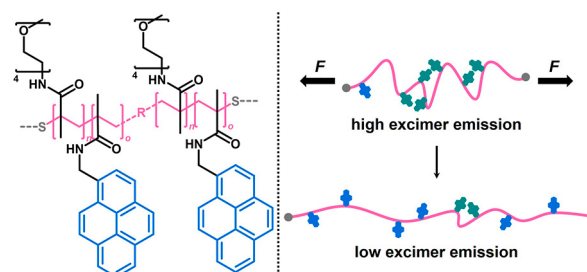


Pyrene-Based Macrocrosslinkers with Supramolecular Mechanochromism for Elastic Deformation Sensing in Hydrogel Networks

Dustin Rasch^{a,b}Robert Göstl^{*a}^a DWI – Leibniz Institute for Interactive Materials, Forckenbeckstr. 50, 52056 Aachen, Germany^b Institute of Technical and Macromolecular Chemistry, RWTH Aachen University, Worringerweg 1, 52074 Aachen, Germany

* goestl@dwI.rwth-aachen.de



Received: 12.08.2022

Accepted after revision: 16.09.2022

DOI: 10.1055/s-0042-1757972; Art ID: OM-2022-08-0030-OA

License terms:

© 2022. The Author(s). This is an open access article published by Thieme under the terms of the Creative Commons Attribution License, permitting unrestricted use, distribution, and reproduction so long as the original work is properly cited. (<https://creativecommons.org/licenses/by/4.0/>).

Abstract Excimer-containing polymers with supramolecular mechanochromism are an attractive and well-investigated class of mechanoresponsive materials. However, only recently steps toward mechanophore-like mechanochromic systems that are anchored within the parent polymer structure and that show defined optical transitions on the molecular scale have been reported. However, the multi-step syntheses of these constructs are tedious. Here we report the development of a series of pyrene-based macrocrosslinkers that display supramolecular mechanochromism and are readily synthesized from mostly commercial reagents. We incorporate the water-soluble macrocrosslinkers in hydrogel networks and demonstrate their reversible mechanochromic behavior in the elastic deformation regime.

Key words: mechanochemistry, mechanochromism, hydrogels

Introduction

Pyrene is a well-established fluorophore¹ that is commonly used because of its ability to form excimers, long excited-state lifetime,² high fluorescence quantum yield, and good photostability.³ Excimer formation is a diffusion-controlled process that leads to a bathochromically shifted emission when a pyrene in the ground state binds to a pyrene in the excited state.⁴ Hence, excimer emission strongly depends on the distance between the excimer-forming molecules rendering pyrene a popular distance-based probe in applications ranging from organic electronics⁵ to sensors for temperature,⁶ pH,⁷ pressure,⁸ small molecules,⁹ protein conformation,¹⁰ lipid structure,¹¹ or nucleic acid recognition.¹²

The strong distance sensitivity of excimer systems is particularly attractive for the visualization of stress and strain in bulk polymer materials.^{13–15} Weder and coworkers have pioneered early research in this field focusing on blending excimer-forming dyes in polymer films.¹⁶ Yet, this has led to only a weak correlation between mechanical polymer deformation and the measured optical signal. While these systems hence have allowed the qualitative observation of force-induced effects, polymer-anchored mechanophore-like^{17,18} systems have only recently been developed that enable the visualization of discrete force-induced molecular events despite the absence of a clear bond dissociation reaction. For example, emitter–quencher pairs have been bridged and anchored within rotaxanes^{19–22} and cyclophanes,²³ and bond torsion with subsequent restructuring of conjugated systems has been demonstrated.^{24–27} However, the multi-step syntheses of these constructs are tedious and occasionally low yielding. Solving this, Weder, Schrettl, and coworkers have developed a readily obtainable folded perylene diimide loop,²⁸ which shows strain-correlated mechanochromism in commodity polymers.²⁹ This has inspired us to investigate whether we could reduce the synthetic complexity of mechanochromic force sensors even further while simultaneously opening up new application fields.

Therefore, we here report the development of a series of pyrene-based macrocrosslinkers (**PyMCs**) with supramolecular mechanochromism, which we incorporate into hydrogels formed with star-shaped poly(ethylene glycol) (sPEG; Figure 1). We achieve this by copolymerization of tetraethylene glycol methyl ether methacrylamide (TEGMEMAAm) and pyrene methacrylamide (PyMAAm) yielding water-soluble **PyMC** chains. We deliberately choose to incorporate **PyMC** into sPEG hydrogels due to their regular network structure leading to outstanding mechanical properties. Unlike randomly crosslinked networks, sPEG hydrogels evenly distribute applied mechanical loads on all bonds and dissipate mechanical energy by controlled uncoiling³⁰ of the network segments.^{31–35} This renders any detection of force-in-

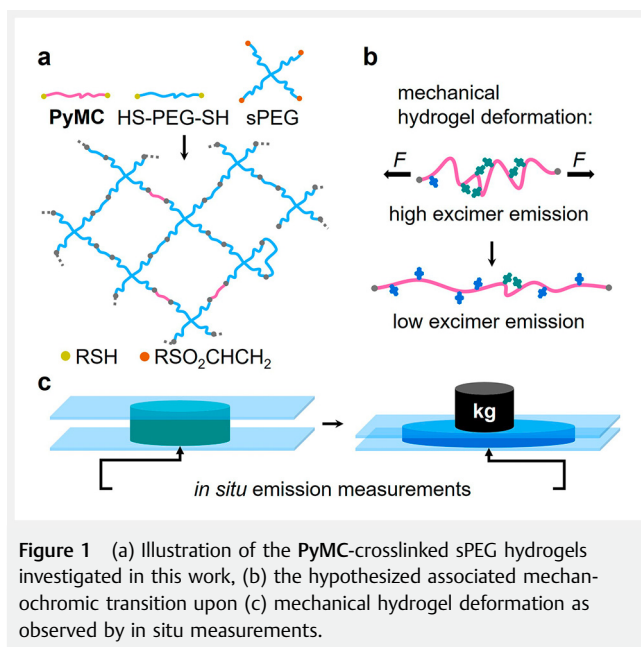


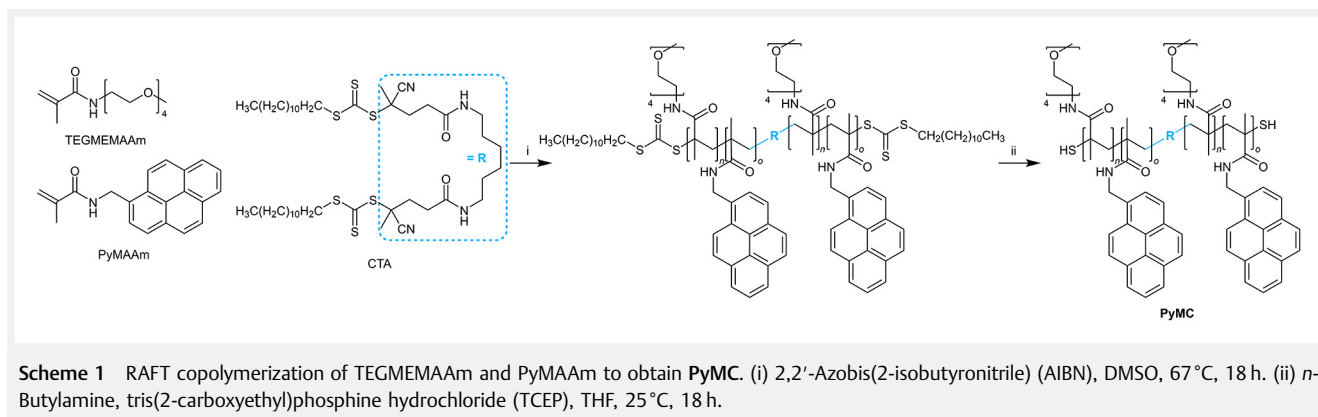
Figure 1 (a) Illustration of the PyMC-crosslinked sPEG hydrogels investigated in this work, (b) the hypothesized associated mechanochromic transition upon (c) mechanical hydrogel deformation as observed by in situ measurements.

duced events using optical force probes³⁶ based on covalent bond scission difficult and hence serves as an ideal proof-of-concept application for our mechanochromic macrocrosslinkers. We show that **PyMC** endows the sPEG hydrogels with reversible mechanochromic behavior in the elastic deformation regime. While pyrene has been investigated as mechanochromic unit in polymers before,^{37–39} the observed emission changes have been fairly small and the conception of distinct macrocrosslinkers and their application in sPEG hydrogels is unknown.

Results and Discussion

Synthesis and Optical Properties of Macrocrosslinkers and Hydrogels

The hydrophobic pyrene units were incorporated into water-soluble **PyMC** chains by reversible addition–fragmentation chain-transfer (RAFT) polymerization starting from a bifunctional chain transfer agent (CTA), the one-step synthesis of which we reported before.⁴⁰ The water-soluble polymers of several widely employed monomers, such as *N*-isopropylacrylamide (NIPAAm) or *N*-vinylcaprolactam (VCL), exhibit lower critical solution temperatures (LCSTs) at 32.0 and 33.5 °C, respectively. Phase separation occurs above the LCST.⁴¹ Since the copolymerization with hydrophobic monomers decreases the LCST (occasionally even below ambient temperature),⁴² the desirable incorporation of high pyrene concentrations for strong fluorescence signals would have been unattainable with most common water-soluble polymers. Therefore, we synthesized copolymers of TEGMEMAAm and PyMAAm by statistical RAFT copolymerization (Scheme 1). We aimed at the incorporation of ca. 70 monomer units resulting in **PyMCs** with a contour length shorter than the commercial 10 kDa HS-PEG-SH employed as a co-crosslinker for hydrogel production. This was to ensure that **PyMC** would be extended first upon mechanically loading the hydrogel. The co-crosslinker was necessary to control the overall pyrene concentration in the hydrogels. The intrinsically high water-solubility of TEGMEMAAm was exploited to maintain a high water-solubility of the **PyMCs** even at high pyrene fractions, which ranged from 1 to 40 mol%. In the following text, the pyrene content of the **PyMCs** in mol% is denoted as subscript, e.g., **PyMC**₄₀ for 40 mol% pyrene. Since the LCST behavior is also concentration-dependent,⁴³ the macrocrosslinkers started to exhibit turbidity at high **PyMC** concentrations from **PyMC**₄₀ upwards. Therefore, **PyMC**₃₂ was identified as an ideal compromise between solubility and a strong fluorescence signal and hence subsequently used for further investigation and the synthesis of the hydrogels.



Expectedly, the ratio of the excimer emission band at 480 nm and the third vibronic monomer emission band at 396 nm (I_E/I_{M3}) increased with increasing **PyMC**₃₂ concentration (Figure 2). In earlier work we found that this was caused by either increasing interchain excimer formation dominating over intrachain excimer formation or by increasing interchain hydrodynamic compression due to passing the overlap concentration.⁴⁰ While **PyMC**₄₀ showed high excimer emission in a broad concentration regime, control **PyMC**₀₁ bearing exactly one pyrene unit per chain showed no excimer emission at all (Scheme S1 and Figure S1).

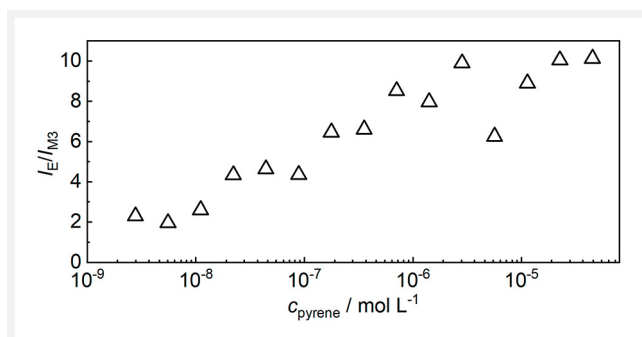


Figure 2 Dependence of **PyMC**₃₂ emission (I_E/I_{M3}) on the macrocrosslinker concentration in H₂O as expressed through the molar pyrene concentration c_{pyrene} . $\lambda_{\text{exc}} = 340$ nm.

Hydrogels were then synthesized using four-arm vinyl sulfone-terminated sPEG ($M_n = 10$ kDa), co-crosslinker HS-PEG-SH ($M_n = 10$ kDa), and **PyMC**₃₂ in H₂O with Et₃N (Figure 1).⁴⁰ The **PyMC**₃₂ concentration was varied while the overall reactant composition was maintained constant by compensation with HS-PEG-SH to maintain identical mechanical properties of the hydrogels. The hydrogels were purified by swelling in a DMSO/THF mixture and subsequent replacement of the solvent with H₂O. To obtain mechanoresponsive hydrogels that use the indicative I_E/I_{M3} ratio as output signal, a suitable **PyMC**₃₂ concentration within the hydrogels must be identified (Figure 3 and Table S1). At low **PyMC**₃₂ concentrations, I_E/I_{M3} converged to a minimum and fluorescence measurements were dominated by noise due to the low pyrene content. With increasing **PyMC**₃₂ concentration, I_E/I_{M3} also increased until the fluorescence spectra were dominated by the excimer emission band and I_{M3} was hardly measurable. For further characterization, we hence chose **PyMC**₃₂ concentrations c_{PyMC} between $2.7 \cdot 10^{-5}$ and $1.4 \cdot 10^{-4}$ mol·L⁻¹ to achieve a reasonable compromise between measurable I_E/I_{M3} ratios and a high overall fluorescence intensity.

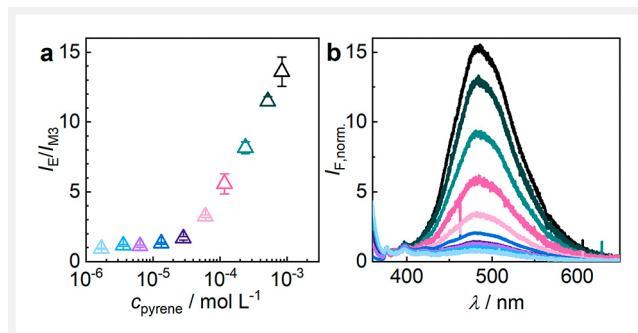


Figure 3 Dependence of **PyMC**₃₂ hydrogel emission on the macrocrosslinker concentration expressed as c_{pyrene} . Hydrogels were swollen to equilibrium. (a) Emission ratio I_E/I_{M3} . Mean values \pm SD from the mean. $N = 5$ independent fluorescence measurements. (b) Individual, normalized (to M3) emission spectra color-coded to the corresponding data points of panel a. $\lambda_{\text{exc}} = 340$ nm. Detailed concentrations are summarized in Table S1.

Photostability of Macrocrosslinkers and Hydrogels

Subsequently, we investigated the photostability of **PyMC**₃₂ and **PyMC**₃₂-crosslinked hydrogels. Pristine pyrene is photostable and not prone to photobleaching.⁴⁴ However, others and we showed that pyrene esters undergo photoinduced solvolysis^{40,45} leading to a rapidly decreasing I_E and increasing I_M featuring an isostilbic point.⁴ We hypothesized that pyrene amides, as in the employed PyMAAm, would not show such behavior. Emission spectra taken over the course of the irradiation of aqueous **PyMC**₃₂ solutions revealed a decrease in I_E (Figure 4a). However, this was significantly slower compared to the photoinduced solvolysis of pyrene esters and showed neither an increase in I_{M3} nor an isostilbic point (Figure 4b). O₂ did not contribute to this process since similar experiments under a N₂ atmosphere showed comparable trends (Figure S2). While the origin of this effect remains unclear, we speculate that it may result from the

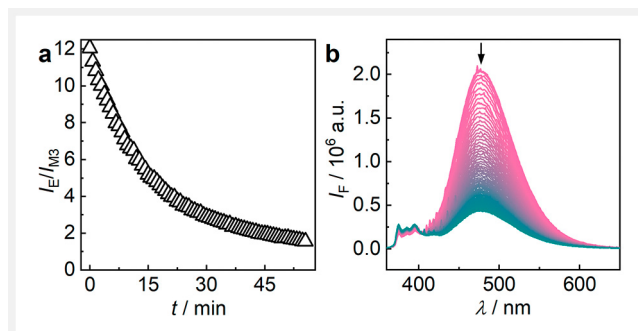


Figure 4 Progress in emission change over time of a **PyMC**₃₂ solution in H₂O upon continuous irradiation at $\lambda = 340$ nm. (a) I_E/I_{M3} in dependence of irradiation time. (b) Individual emission spectra corresponding to the data points of panel a. $\lambda_{\text{exc}} = 340$ nm.

complex interactions of pyrene in hydrophilic environments. Excimer formation is usually the result of diffusion-controlled interaction of a pyrene in the ground state with a pyrene in the excited state.⁴⁶ Pyrene was shown to form preassociated excimers in aqueous environments.⁴⁴ The excitation of such preassociates may lead to a separation of the ground and excited state pyrenes, which may cause the loss of excimer emission. However, we found that this effect was very slow in hydrogels and hence negligible in the investigated timeframes for mechanical analysis (Figure 5).

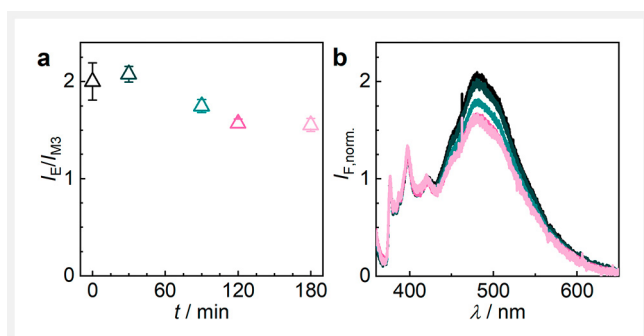


Figure 5 Progress in emission change over time of a **PyMC₃₂** ($\rho_{\text{PyMC}} = 2.45 \cdot 10^{-5} \text{ g} \cdot \text{L}^{-1}$) hydrogel upon continuous irradiation at $\lambda = 340 \text{ nm}$. Hydrogel was swollen to equilibrium. (a) I_E/I_{M3} in dependence of irradiation time. Mean values \pm SD from the mean. $N = 5$ independent fluorescence measurements. (b) Individual, normalized (to M3) emission spectra color-coded to the corresponding data points of panel a. $\lambda_{\text{exc}} = 340 \text{ nm}$.

Influence of the Degree of Swelling on Hydrogel Emission

In addition to the **PyMC** concentration, we investigated the influence of the degree of swelling (d_s) on the I_E/I_{M3} ratio, which was calculated from the masses of the dry polymer (m_d) and of added H_2O (m_w) using Equation 1. Equilibrium swelling was reached when the sample mass was constant for 3 d upon immersion in excess H_2O . We used a hydrogel with a **PyMC₃₂** mass concentration of $\rho_{\text{PyMC}} = 2.08 \cdot 10^{-4} \text{ g} \cdot \text{L}^{-1}$ (Figure 6). Only little variation of I_E/I_{M3} upon varying d_s occurred in the investigated swelling regime from 1000 to 8000%. However, we found in earlier work that considerably dried hydrogels with a very low d_s reached a threshold value where I_E/I_{M3} decreased steeply to almost no excimer emission at all caused by the dissolution of preassociated pyrene within the polymer backbone.⁴⁰ This implied that it was critical to prevent the hydrogels from drying out over the course of the performed measurements. Since we observed that mechanical testing in uniaxial extension mode led to rapid drying effects, we hence performed subsequent mechanical testing in uniaxial compression mode.

$$d_s = \frac{m_w}{m_d} \cdot 100$$

Equation 1 Formula used to calculate the degree of swelling of the hydrogels in %.

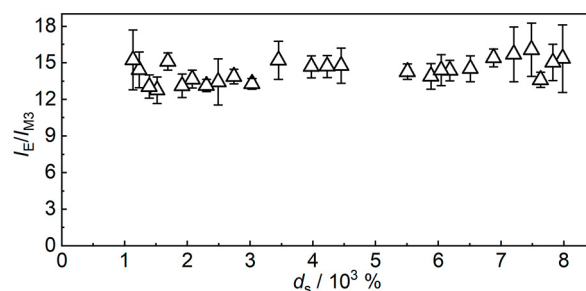


Figure 6 Dependence of **PyMC₃₂** ($\rho_{\text{PyMC}} = 2.08 \cdot 10^{-4} \text{ g} \cdot \text{L}^{-1}$) hydrogel emission ratio I_E/I_{M3} on the degree of swelling d_s with H_2O . Mean values \pm SD from the mean. $N = 5$ independent fluorescence measurements. $\lambda_{\text{exc}} = 340 \text{ nm}$.

Mechanochromic Hydrogel Response

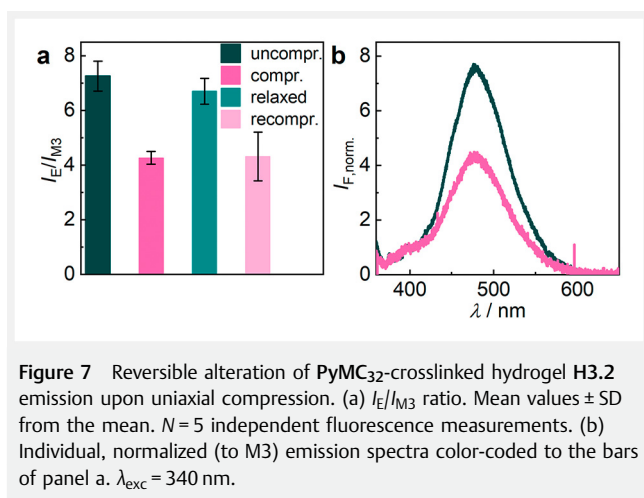
To investigate the mechanochromic properties of the **PyMC₃₂** hydrogels, we used three different variants with ρ_{PyMC} ranging from 0.025 to 0.129 $\text{g} \cdot \text{L}^{-1}$. Since the network segments of the hydrogels at equilibrium d_s were already subject to maximum uncoiling and hence became rather brittle, we decided to investigate each of the three hydrogel samples at three distinct d_s below equilibrium d_s . The resulting nine investigated samples are denoted **H1.1** to **H3.3** and their associated ρ_{PyMC} , c_{pyrene} , and d_s can be found in Table 1.

Table 1 List of **PyMC₃₂**-crosslinked hydrogels **H1.1** to **H3.3** and their associated **PyMC₃₂** mass concentrations ρ_{PyMC} , pyrene molar concentrations c_{pyrene} , and investigated degrees of swelling d_s .^a

No.	$\rho_{\text{PyMC}}/\text{g} \cdot \text{L}^{-1}$	$c_{\text{pyrene}}/10^{-5} \text{ mol} \cdot \text{L}^{-1}$	$d_s/\%$
H1.1	0.026	2.66	1352
H1.2	0.025	2.72	2804
H1.3	0.026	2.77	4255
H2.1	0.049	5.26	1352
H2.2	0.055	5.88	2804
H2.3	0.050	5.37	4255
H3.1	0.129	13.81	1352
H3.2	0.120	12.71	2804
H3.3	0.129	13.85	4255

^a ρ_{PyMC} and c_{pyrene} were calculated with respect to the equilibrium d_s .

To circumvent the drying effect observed under uniaxial extension, we placed the hydrogel samples between two glass plates and subjected these to maximum compression using a micrometer screw stopping shortly before the glass plates broke (Figure 7). For example, upon compression of **H3.2**, I_E/I_{M3} decreased from 7.2 to 4.3 corresponding to a relative change of ca. 40%. Notably, I_E/I_{M3} recovered almost fully after de-loading the hydrogel. Renewed compression then proved the reversibility of this effect measured up to 13 times (Figure S3). Importantly, we observed the mechanochromic changes in the elastic deformation regime highlighting the advantage of the excimer-based supramolecular force sensors over traditional bond scission-based optical force probes for application in soft but elastically very extendible materials.



The results were qualitatively similar for all investigated hydrogels (Figure 8) where deviations were observed mainly in the relative change of I_E/I_{M3} upon compression ranging from 20 to 50%. Notably, these relative changes are considerably higher than those reported to the literature before.^{37–39} We believe that the molecular origin of the me-

chanochromic behavior is the uncoiling and gliding of **PyMC** during hydrogel compression (and thereby lateral extension). We hypothesize that the preassociated intra- and intermolecular pyrene aggregates are broken and an increase in pyrene monomer emission is consequently observed.

Since **H2** showed the largest relative changes, we subsequently used this hydrogel batch for further mechanical testing. **H2.2** was loaded 3 \times with different defined weights. The engineering stress σ was calculated from the ratio of the force F exerted by the weight and the initial surface area of the hydrogel A_0 . It became clear that I_E/I_{M3} decreased with increasing σ (Figure 9). Although σ correlated to I_E/I_{M3} , the relation was non-linear. The largest changes were observed in the initial stages of the elastic deformation. At higher stresses, the relative change in I_E/I_{M3} appeared to reach a limiting value. Mechanistically, this may be explained by the maximum possible displacement of the preassociated pyrenes from their equilibrium where residual excimer emission was caused by interchain pyrene interactions.

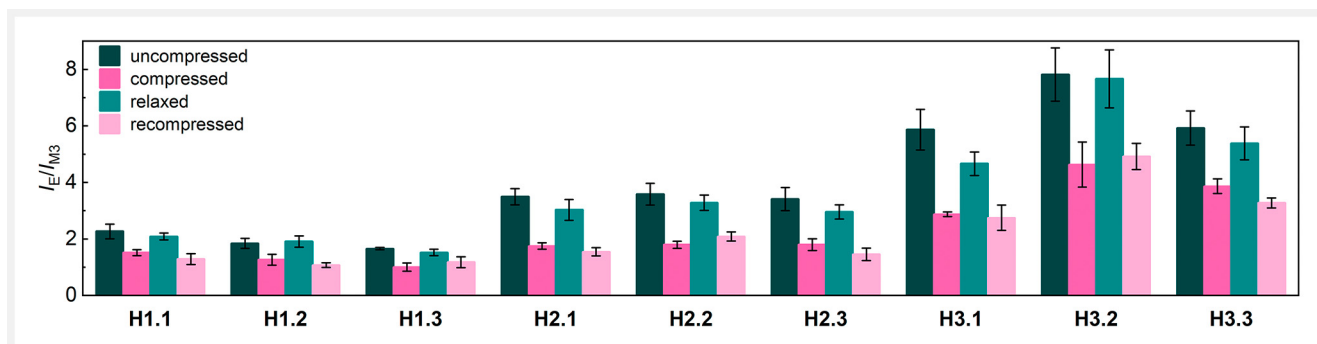
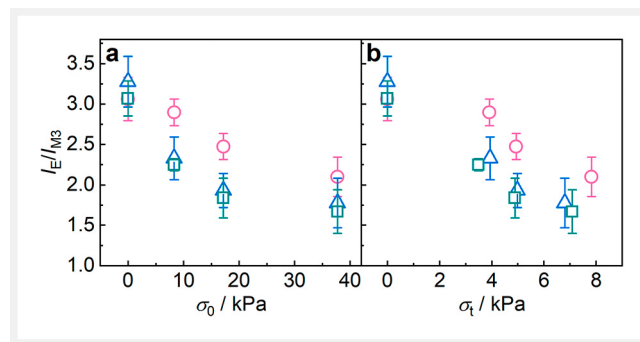


Figure 8 Reversible alteration of PyMC₃₂-crosslinked hydrogels **H1.1** to **H3.3** I_E/I_{M3} ratio upon uniaxial compression. Mean values \pm SD from the mean. $N = 5$ independent fluorescence measurements. $\lambda_{exc} = 340$ nm.

Conclusions

We have shown the straightforward synthesis of **PyMC** macrocrosslinkers that display supramolecular mechanochromism. **PyMCs** were obtained in a two-step reaction from monomers that are commercial or can likewise be prepared in a one-step reaction. From these, we prepared sPEG-based hydrogels. We fully characterized the fluorescence properties and photostability of **PyMCs** in solution and in hydrogels depending on concentration effects and degree of swelling. We then presented the reversible mechanochromic behavior of the sPEG hydrogels in the elastic deformation regime. Thereby, we provide a protocol for the facile synthesis of mechanochromic hydrogels and anticipate that this will incentivize easier entry into the field for non-chemical researchers.

Experimental Section

Materials. The bifunctional CTA was synthesized in one step according to our previously published protocol.⁴⁰ Et₃N (99.5%, dry, 121-44-8), 4-(dimethylamino)pyridine (99%, DMAP, 1122-58-3), 1,6-diaminohexane (98%, 124-09-4), methacryloyl chloride (97%, 920-46-7), and AIBN (98%, 78-67-1) were obtained from Merck. AIBN was recrystallized from hexane before use. CH₂Cl₂ (99.9%, dry, 75-09-2), THF (99.9%, 109-99-9), MeOH (99.9%, 67-56-1), EtOAc (99.8%, 141-78-6), and DMF (99.8%, 68-12-2) were obtained from Acros Organics. 2,5,8,11-Tetraoxatridecan-13-amine (98%, 85030-56-4), pyren-1-ylmethanaminium chloride (97%, 93324-65-3), and TCEP (99%) were bought from abcr. Dialysis membranes were bought from Spectrum Labs (MWCO: 10 kDa). SH-PEG-SH ($M_n = 10$ kDa, $X_n = 222$, 99%) and 4-arm vinylsulfone-terminated sPEG ($M_n = 10$ kDa, 99%) were obtained from Creative PEGworks.

Methods. NMR spectra were recorded at room temperature in CDCl₃ on a 400 MHz Bruker Avance 400 (¹³C: 101 MHz). Chemical shifts were reported in δ units using residual protonated solvent signals as the internal standard. Mass spectrometry was conducted with HRMS Bruker microOTOF-Q II employing electron spray ionization ESI⁺. MeOH:H₂O:HCOOH = 80:20:0.1 was used as a solvent. Molar masses (M_n and M_w) and dispersities (\mathcal{D}_M) were determined by gel permeation chromatography (GPC). Samples were filtered through a CHROMAFIL PTFE membrane with 0.45 μ m pore size. GPC with THF ($\geq 99.7\%$, unstabilized, HiPerSolv CHROMANORM[®] HPLC grade, VWR) as the eluent: HPLC pump (1260 Infinity II, Agilent), a refractive index (RI) (1290 Infinity II, Agilent), a UV- (UV-2075plus, Jasco) and a multi-angle light scattering detector (SLD 7100, Polymer Standards Service). The samples contained 250 mg·mL⁻¹ 3,5-di-*tert*-4-butylhydroxytoluene (BHT, $\geq 99\%$, Fluka) as the internal standard. 1 pre-column (8 \times 50 mm) and 4

SDplus gel columns (8 \times 300 mm, MZ Analysentechnik) were applied at a flow rate of 1.0 mL·min⁻¹ at 20 °C. The diameter of the gel particles measured 5 μ m, and the nominal pore widths were 50, 10², 10³, and 10⁴ Å. GPC with DMF ($\geq 99.9\%$, HiPerSolv CHROMANORM[®] HPLC grade, VWR) as the eluent: HPLC pump (1260 Infinity, Agilent), a dual RI/Visco (ETA-2020, WGE), and a UV-detector (VWD, 1290 Infinity II, Agilent). The eluent contained 1 g·L⁻¹ LiBr ($\geq 99\%$, Sigma-Aldrich). The samples contained 2 μ L·mL⁻¹ toluene ($\geq 99\%$, Sigma-Aldrich) as the internal standard. One pre-column (8 \times 50 mm) and three GRAM gel columns (8 \times 300 mm, Polymer Standards Service) were applied at a flow rate of 1.0 mL·min⁻¹ at 60 °C. The diameter of the gel particles measured 10 μ m, the nominal pore widths were 30, 10², and 10³ Å. Calibration was performed using narrowly distributed poly(methyl methacrylate) standards (Polymer Standards Service). Results were evaluated using the PSS WinGPC UniChrom software (version 8.3.2).

Procedures

Optical experiments. UV-vis absorption spectroscopy was performed on a Thermo Scientific Evolution 300 and fluorescence spectroscopy on a Horiba Fluoromax-4P at room temperature in H₂O (VWR, HPLC grade) and THF (VWR, Reag. Ph Eur). Excitation and emission spectra of the hydrogels were recorded with a compact spectrometer (CCS200, Thorlabs). A fiber-coupled LED (M340F3, Thorlabs) was used as a light source. The emission was detected simultaneously with the excitation with a fiber Y-bundle reflection probe (RP24, Thorlabs), which also transmitted the excitation light. The spectra were analyzed with the Thorlabs OSA software (version 2.90).

Compression experiments. A rectangular hydrogel sample (ca. 5 \times 5 mm) was cut out by a scalpel. This was placed on the surface of a microscopy-grade glass slide and the surface area was determined with a caliper. Afterwards, the sample was covered with a second glass slide and placed on a pedestal. Force was applied by placing defined metal weights on top of the cover slide. The deformed hydrogel increased in surface but did not exit the glass slide edges. The compressed surface area was determined again with a caliper through the bottom glass slide.

Synthesis of TEGMEMAAm. 2,5,8,11-Tetraoxatridecan-13-amine (0.91 g, 4.40 mmol) was dissolved in dry THF (20 mL) with DMAP (0.108 g, 0.88 mmol). The flask was flushed with Ar for 7 min and then dry Et₃N (0.39 mL, 5.29 mmol) was added. Then, methacryloyl chloride (0.33 mL, 4.85 mmol) was added dropwise at 0 °C under Ar. The reaction was stirred and slowly warmed to r.t. overnight. The reaction was quenched with aq. Na₂CO₃ solution and then extracted with CH₂Cl₂. The organic layer was washed with 0.1 M aq. HCl, brine, and then dried over MgSO₄. The solvent was

evaporated in vacuo and the product was purified by silica column chromatography with EtOAc and MeOH (95:5, $R_f=0.35$). A yellow oil was obtained (87%). **¹H NMR** (CDCl₃): δ (ppm): 6.50 (s, 1 H, NH), 5.70 (s, 1 H, vinyl), 5.30 (s, 1 H, vinyl), 3.60 (m, 18 H, -O-CH₂-CH₂-O-), 3.36 (s, 3 H, O-CH₃), 1.96 (s, 3 H, CH₃). See Figure S7. **¹³C NMR** (CDCl₃): 120.0, 72.4, 71–70, 59.5, 39.9, 19.1. See Figure S8. **HRMS** (ESI⁺): m/z calcd. for C₁₃H₂₅NNaO₅⁺: 298.1625; found: 298.1495. See Figure S9.

Synthesis of PyMAAm. Pyren-1-ylmethanaminium chloride (2.46 g, 10.20 mmol) was added to a reaction flask, dried in vacuo, and then suspended in dry THF (100 mL). By adding DMAP (0.25 g, 2.04 mmol) and Et₃N (3.11 mL, 22.40 mmol), the suspension slowly dissolved. The reaction mixture was stirred for 30 min. Then, methacryloyl chloride was added dropwise at 0 °C and the reaction was stirred at r.t. overnight. The reaction was then diluted with EtOAc and extracted 3× with 0.1 M aq. HCl and 3× with brine. The organic layer was dried over MgSO₄, collected, and the solvent was evaporated. The product was purified by silica column chromatography with CH₂Cl₂ and EtOH (97:3, $R_f=0.5$) yielding a white-yellow solid (91%). **¹H NMR** (CDCl₃): δ (ppm): 8.05 (m, 9 H, aromatic), 6.12 (s, 1 H, NH), 5.69 (s, 1 H, vinyl), 5.32 (s, 1 H, vinyl), 5.21 (m, 2 H, -CH₂-N-), 1.98 (s, 3 H, -CH₃). See Figure S10. **¹³C NMR** (CDCl₃): 140.3, 131.8–129.6, 125.5, 125.2, 120.2, 42.7, 19.2. See Figure S11. **HRMS** (ESI⁺): m/z calcd. for C₂₁H₁₈NO⁺: 300.1383; found: 300.1248. See Figure S12.

General procedure for PyMC synthesis. The bifunctional CTA (1 equiv.) was used in statistical copolymerizations of PyMAAm (2·*o* equiv.) and TEGMEMAAm (2·*n*=70–2·*o* equiv.) in dry DMSO (66 wt%), cf. Scheme 1. To this, AIBN (0.4 equiv.) was added, and the solution was kept at 67 °C for 18 h achieving conversions >90% as determined by ¹H NMR. The obtained polymers were dialyzed against THF and then against H₂O. Yellow polymers were obtained with typical yields of ~90%. The polymers were analyzed by ¹H NMR and GPC (Figures S17–S19). The feed fraction of PyMAAm during polymerization was slightly higher than the incorporated fraction that was found in the polymer. Afterwards, the terminal trithiocarbonates were aminolyzed by the addition of *n*-butylamine (30 equiv.) under Schlenk conditions in THF (0.012 mol·L⁻¹) in the presence of TCEP (ca. 1 mg). Hereafter, the polymer was dialyzed against THF and then H₂O, dried in vacuo, and colorless **PyMCs** were received. \bar{D}_M was typically ~1.3 (Figure S18).

General procedure for hydrogel preparation. Polymerization was performed by step-growth polymerization of **PyMC** macrocrosslinkers (*z* equiv.) alongside HS-PEG-SH (2·*z* equiv., 10 kDa) and 4-armed sPEG terminally functionalized with 4× vinyl sulfone (1 equiv.) via a thiol-ene reaction at pH=8–10. Exemplarily, sPEG (1.3 μmol, 6.60 mg), HS-PEG-SH (2.66 μmol, 26.66 mg), and **PyMC** (0.068 mg) were dissolved in H₂O (200 μL) and cast into a PTFE-coated

metal mold. After the addition of Et₃N (30 μL), the mold was covered and left to react overnight. The hydrogels were immersed first in DMSO/THF then in H₂O to remove residual reactants yielding transparent hydrogels with visible blue or green fluorescence based on the identity and fraction of the incorporated **PyMC**.

Funding Information

D. R. and R. G. are grateful for support by a Freigeist-Fellowship of the Volkswagen Foundation (92888). Parts of the analytical investigations were performed at the Center for Chemical Polymer Technology CPT, which was supported by the European Commission and the federal state of North Rhine-Westphalia (300088302).

Supporting Information

Supporting Information for this article is available online at <https://doi.org/10.1055/s-0042-1757972>.

Primary Data

Primary Data for this article are available online at <https://zenodo.org/record/6984827>.

Conflict of Interest

The authors declare no conflict of interest.

References

- (1) Förster, T.; Kasper, K. Z. *Elektrochem. Ber. Bunsenges. Phys. Chem.* **1955**, *59*, 976.
- (2) Birks, J. B.; Dyson, D. J.; Munro, I. H.; Flowers, B. H. *Proc. R. Soc. London, Ser. A* **1963**, *275*, 575.
- (3) de Halleux, V.; Mamdouh, W.; De Feyter, S.; De Schryver, F.; Levin, J.; Geerts, Y. H. *J. Photochem. Photobiol., A* **2006**, *178*, 251.
- (4) Förster, T. *Angew. Chem. Int. Ed. Engl.* **1969**, *8*, 333.
- (5) Figueira-Duarte, T. M.; Müllen, K. *Chem. Rev.* **2011**, *111*, 7260.
- (6) Pietsch, C.; Vollrath, A.; Hoogenboom, R.; Schubert, U. S. *Sensors* **2010**, *10*, 7979.
- (7) Dembska, A.; Juskowiak, B. *Spectrochim. Acta, Part A* **2015**, *150*, 928.
- (8) Claucherty, S.; Sakaue, H. *Sens. Actuator, A* **2021**, *317*, 112359.
- (9) Kovalev, I. S.; Taniya, O. S.; Slovesnova, N. V.; Kim, G. A.; Santra, S.; Zyryanov, G. V.; Kopchuk, D. S.; Majee, A.; Charushin, V. N.; Chupakhin, O. N. *Chem. Asian J.* **2016**, *11*, 775.
- (10) Bains, G.; Patel, A. B.; Narayanaswami, V. *Molecules* **2011**, *16*, 7909.
- (11) Somerharju, P. *Chem. Phys. Lipids* **2002**, *116*, 57.

- (12) Krasheninina, O. A.; Novopashina, D. S.; Apartsin, E. K.; Venyaminova, A. G. *Molecules* **2017**, *22*, 2108.
- (13) Sagara, Y.; Yamane, S.; Mitani, M.; Weder, C.; Kato, T. *Adv. Mater.* **2016**, *28*, 1073.
- (14) Calvino, C.; Neumann, L.; Weder, C.; Schrettl, S. *J. Polym. Sci., Part A: Polym. Chem.* **2017**, *55*, 640.
- (15) Traeger, H.; Kiebal, D. J.; Weder, C.; Schrettl, S. *Macromol. Rapid Commun.* **2021**, *42*, 2000573.
- (16) Löwe, C.; Weder, C. *Adv. Mater.* **2002**, *14*, 1625.
- (17) O'Neill, R. T.; Boulatov, R. *Nat. Rev. Chem.* **2021**, *5*, 148.
- (18) Chen, Y.; Mellot, G.; Luijk, D. van; Creton, C.; Sijbesma, R. P. *Chem. Soc. Rev.* **2021**, *50*, 4100.
- (19) Sagara, Y.; Karman, M.; Verde-Sesto, E.; Matsuo, K.; Kim, Y.; Tamaoki, N.; Weder, C. *J. Am. Chem. Soc.* **2018**, *140*, 1584.
- (20) Muramatsu, T.; Sagara, Y.; Traeger, H.; Tamaoki, N.; Weder, C. *ACS Appl. Mater. Interfaces* **2019**, *11*, 24571.
- (21) Sagara, Y.; Karman, M.; Seki, A.; Pannipara, M.; Tamaoki, N.; Weder, C. *ACS Cent. Sci.* **2019**, *5*, 874.
- (22) Muramatsu, T.; Okado, Y.; Traeger, H.; Schrettl, S.; Tamaoki, N.; Weder, C.; Sagara, Y. *J. Am. Chem. Soc.* **2021**, *143*, 9884.
- (23) Sagara, Y.; Traeger, H.; Li, J.; Okado, Y.; Schrettl, S.; Tamaoki, N.; Weder, C. *J. Am. Chem. Soc.* **2021**, *143*, 5519.
- (24) van de Laar, T.; Schuurman, H.; van der Scheer, P.; Maarten van Doorn, J.; van der Gucht, J.; Sprakel, J. *Chem* **2018**, *4*, 269.
- (25) Raisch, M.; Maftuhin, W.; Walter, M.; Sommer, M. *Nat. Commun.* **2021**, *12*, 4243.
- (26) Raisch, M.; Reiter, G.; Sommer, M. *ACS Macro Lett.* **2022**, *11*, 760.
- (27) Hu, H.; Cheng, X.; Ma, Z.; Sijbesma, R. P.; Ma, Z. *J. Am. Chem. Soc.* **2022**, *144*, 9971.
- (28) Traeger, H.; Sagara, Y.; Kiebal, D. J.; Schrettl, S.; Weder, C. *Angew. Chem. Int. Ed.* **2021**, *60*, 16191.
- (29) Traeger, H.; Sagara, Y.; Berrocal, J. A.; Schrettl, S.; Weder, C. *Polym. Chem.* **2022**, *13*, 2860.
- (30) Liese, S.; Gensler, M.; Krysiak, S.; Schwarzl, R.; Achazi, A.; Paulus, B.; Hugel, T.; Rabe, J. P.; Netz, R. R. *ACS Nano* **2017**, *11*, 702.
- (31) Lutolf, M. P.; Hubbell, J. A. *Biomacromolecules* **2003**, *4*, 713.
- (32) Rehmann, M. S.; Skeens, K. M.; Kharkar, P. M.; Ford, E. M.; Mavrerakis, E.; Lee, K. H.; Kloxin, A. M. *Biomacromolecules* **2017**, *18*, 3131.
- (33) Wang, J.; Zhang, F.; Tsang, W. P.; Wan, C.; Wu, C. *Biomaterials* **2017**, *120*, 11.
- (34) Licht, C.; Rose, J. C.; Anarkoli, A. O.; Blondel, D.; Roccio, M.; Haraszti, T.; Gehlen, D. B.; Hubbell, J. A.; Lutolf, M. P.; De Laporte, L. *Biomacromolecules* **2019**, *20*, 4075.
- (35) Grad, E. M.; Tunn, I.; Voerman, D.; de Léon, A. S.; Hammink, R.; Blank, K. G. *Front. Chem.* **2020**, *8*, 536.
- (36) He, S.; Stratigaki, M.; Centeno, S. P.; Dreuw, A.; Göstl, R. *Chem. Eur. J.* **2021**, *27*, 15889.
- (37) Rossi, N. A. A.; Duplock, E. J.; Meegan, J.; Roberts, D. R. T.; Murphy, J. J.; Patel, M.; Holder, S. J. *J. Mater. Chem.* **2009**, *19*, 7674.
- (38) Roberts, D. R. T.; Patel, M.; Murphy, J. J.; Holder, S. J. *Sens. Actuators, B* **2012**, *162*, 43.
- (39) Cellini, F.; Block, L.; Li, J.; Khapli, S.; Peterson, S. D.; Porfiri, M. *Sens. Actuators, B* **2016**, *234*, 510.
- (40) Rasch, D.; Göstl, R. *ACS Polym. Au* **2021**, *1*, 59.
- (41) Roy, D.; Brooks, W. L. A.; Sumerlin, B. S. *Chem. Soc. Rev.* **2013**, *42*, 7214.
- (42) Schild, H. G. *Prog. Polym. Sci.* **1992**, *17*, 163.
- (43) Chua, G. B. H.; Roth, P. J.; Duong, H. T. T.; Davis, T. P.; Lowe, A. B. *Macromolecules* **2012**, *45*, 1362.
- (44) Winnik, F. M. *Chem. Rev.* **1993**, *93*, 587.
- (45) Iwamura, M.; Ishikawa, T.; Koyama, Y.; Sakuma, K.; Iwamura, H. *Tetrahedron Lett.* **1987**, *28*, 679.
- (46) Birks, J. B. *Nature* **1967**, *214*, 1187.